PHYSICSAccess Research Paper
ISSN Online: 2756-3898, ISSN Print: 2714-500X https://doi.org/10.47514/phyaccess.2024.4.1.002

# Structural, Electronic, and Optical Properties of Stanene and Stanene-Doped Non-metals for Optoelectronics Applications: A first-principle Study

**Abdulkadir S Gidado[1], Lawal Abubakar[1], Lawan S Taura[2], Abdullahi Lawal[3] and Abdulmalik Isah[1]**

[1] Department of Physics, Bayero University Kano, Kano State, Nigeria
[2] Department of Physics, Sule Lamido University Kafin Hausa, Jigawa State, Nigeria
[3] Department of Physics, Federal University Dutse, Jigawa State, Nigeria

Corresponding E-mail: abubakarlawall1122@gmail.com

Received 10-04-2024
Accepted for publication 29-04-2024
Published 30-04-2024

## Abstract

In this paper, the structural, electronic, and optical properties of sulfur and phosphorus-doped stanene were investigated using the density functional theory (DFT) projected augmented wave (PAW) method. Native stanene has a zero-band gap but when doped with sulfur and phosphorus atoms, it results in a direct band gap opening. Specifically, the bands of stanene doped with 25.0% sulfur and 25.0% phosphorus are 0.77 eV and 0.47 eV compared to other doping concentrations. Optical analysis shows anisotropic behavior in stanene-doped phosphorus and sulfur with higher refractive indices than native stanene. This suggests that $SnP_{12.5\%}$, $SnP_{25.0\%}$, $SnS_{12.5\%}$ and $SnS_{25.0\%}$ are promising for optoelectronic applications.

Keywords: 2D Materials; Band Structure; DFT; Inversion Symmetry; Topological Insulators.

## I. Introduction

Two-dimensional layered semiconducting nanomaterials comprising silicene, germanene, graphene, stanene, and transition metal dichalcogenides are valuable materials that are needed for the study of low-dimensional physics. Due to their astonishing and distinctive crystal structures, they serve as the building blocks in the construction of integrated multifunctional devices [1]. To advance developments in low-power and high-speed optoelectronic devices for practical applications, 2D semiconducting materials with good band gaps and high carrier mobility are needed. A few years back, several 2D materials have been extensively studied and developed such as graphene, silicene, and germanene. Hexagonal honeycomb lattices formed by other group-IV elements such as Si, Ge, and Sn have been attracting increasing attention on account of their potential facilitated integration and application in the semiconductor industry [2].

Stanene is a two-dimensional sheet composed of tin (Sn) atoms arranged in a honeycomb lattice, similar to graphene. Ab initio calculations indicate that, unlike graphene, a low-buckled configuration of stanene is more stable compared to the planar geometry [3]. The first principle simulations indicate that stanene's low buckling structure is projected to be more stable and to reflect a big gap in the quantum spin hall state [4]. The fact that stanene retains its time-reversal symmetry and inversion even after spin-orbit coupling (SOC) is included is one of its key characteristics. However, when

 

the inversion symmetry breaks, it shows splitting in its energy band structure [5]. Stanene and its derivatives can support a large gap QSH state and also provide enhanced thermoelectricity, topological superconductivity, giant magnetoresistance, perfect spin filter, and quantum anomalous hall (QAH) effect near room temperature, which utilize strain engineering, functional group decoration, and the substrate [6].

As one of the most important honeycomb-like structures, stanene also exhibits fascinating properties such as Dirac-cone-shaped energy band structure and ultra-high carrier mobility but has an unfortunate zero-band-gap nature [7]. Consequently, the zero-band gap nature of stanene limits its technological applications. The zero-band gap nature of stanene in the absence of spin-orbit coupling can be verified via first-principles calculations. However, in recent years, several studies through elemental doping which prove to be more effective have been carried out to engineer the band gap of 2D materials via density functional theory [8]. The structural and electronic properties of two-layered stanene and graphene heterostructure (Sn/G) were studied by utilizing first-principle calculations, they found that interlayer collaborations in stanene and graphene heterostructure can initiate tunable band gaps at stanene's Dirac point, and frail p-type and n-type doping of stanene and graphene, separately, creating a modest quantity of electron move from stanene to graphene [9]. Also, the first-principle study was utilized to investigate the structural stability and electrical properties of the Sn/BeO heterostructure. The results from computations show that the introduction of BeO not only leads to a significant band gap opening of 98.0 meV but also maintains the various intrinsic electrical properties of stanene to a large extent [10].

Since pristine stanene exhibits a zero band gap nature which then limits its applications in the semiconductor industry, we therefore in this paper, adopt the method of substitutional doping of stanene monolayer sheets using non-metals (Phosphorus and Sulfur are materials that are abundant, very cheap, form good bonds with group iv elements, and are non-toxic) to open up its band gap and as well investigate the band structure, dielectric function, electron energy loss function, refractive index, reflectivity, and extinction coefficient via the framework of density functional theory as implemented in the quantum expresso code. A similar approach was used by [11] on graphene. And [12] on stanene-doped Alkali earth metals. Fig. 1 shows the optimized structure of pristine stanene concerning their bond length, bond angle, and buckling height.

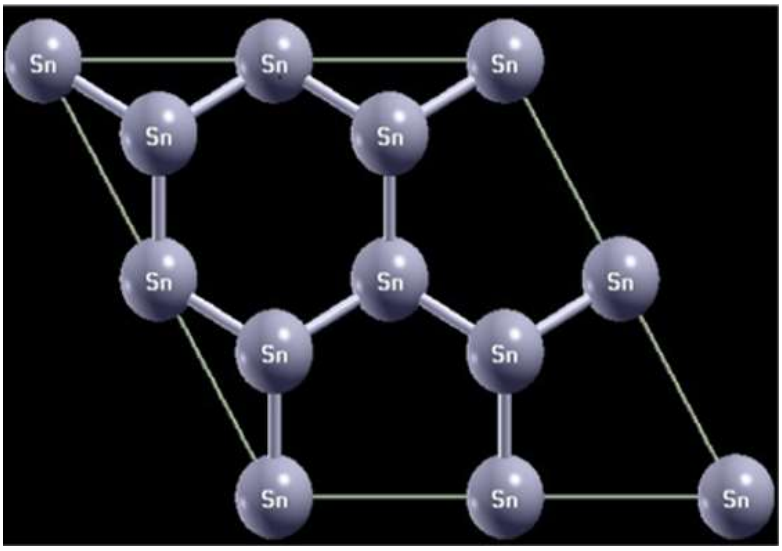


Fig. 1 Optimized structure of pristine stanine.

## II. Theoretical Background

A quantum mechanical theory called density functional theory (DFT) is applied in physics and chemistry to study the electronic structure of many-body systems, specifically atoms, molecules, and condensed phases. It is primarily employed to study the ground state of these systems. With this theory, the properties of a many-electron system can be determined by using functionals, i.e., functions of another function, which in this case is the electron density. Over the past 20 years, density functional theory (DFT) has become a much-used tool in most branches of chemistry and physics. Such computations are frequently made as part of experimental investigations in organic and inorganic chemistry, employing a widely used code, a standard foundation, and a standard functional approximation. Similar changes are currently taking place in the field of materials science, where over the last ten years, advancements in hardware and software have made it feasible to conduct systematic comparisons with experiments on a wide variety of materials, discovering which approximations

are accurate and why, and enabling accurate property predictions based on first principles.[13]. Density functional theory (DFT) was first introduced by Hohenberg and Kohn in 1964. This introduction entailed the following theorem that they established: (i) Except an additive constant, an external potential v(r) and the electron-electron Coulomb repulsion applied to any number of electrons in a box represent a unique functional of the electron density n(r). (ii) The Density that minimizes the total energy is the exact ground state density. The following expressions or equations for the potential, the density, and functionals, both signify that the position variable is a vector [14]. The Hamiltonian of the system is written as.

$$H = T + U \quad (1)$$

$$V = \int v(r)\varphi * (r)\varphi(r)dr \quad (2)$$

The electron-electron interaction $U_{e-e}$ also known as the coulomb potential operator is given by.

$$U(r) = \frac{1}{2}\sum_{i \neq r}\frac{e\wedge 2}{|r_i - r_j|} \quad (3)$$

The kinetic energy operator T of the system is given by.

$$T = \frac{-\hbar\wedge 2}{2Me}\sum_i \nabla \mathrm{i} \wedge 2 \quad (4)$$

They concluded that the sum of the kinetic and electron-electron interaction energies is a universal function of the charge density since Ψ is a function of n(r).

$$F[n(r)] = (\varphi, (T + U)\varphi) \quad (5)$$

The foregoing results indicated that we have the energy functional for a given potential v(r).

$$E[n] = \int v(r)n(r)dr + F[n] \quad (6)$$

Hohenberg and Kohn went on to show that with the proper ground state density n(r), this special density function reaches its minimum (from above), given the total number of particles, is kept constant.

$$N[n] = \int n(r)dr \quad (7)$$

Specifically, the actual quote from the Hohenberg and Kohn article follows; "It is well known that for a system of N particles, the energy functional of Ψ′ has a minimum at the 'correct' ground state Ψ, relative to arbitrary variations of Ψ′ in which the total number of particles is kept constant."

$$E[\varphi'] = (\varphi' V\varphi) + (\varphi'(T + U)\varphi) \quad (8)$$

## III. Computational Method

In this work, the simulations were carried out using density functional theory based on first principle calculations as implemented in the QUANTUM ESPRESSO code [15]–[16]. Within the framework of the Generalized gradient approximation (GGA) coupled with the Perdew- Burke-Ernzerhof (GGA-PBE) exchange-correlation functional method which was adopted to carry out the electronic structure calculations. Functionals such as the PBE are used for the core correction of electrons. As for the electronic wave function description, the projected augmented wave (PAW) method was used. For maximum accuracy, a self-consistent convergence was achieved for all calculations. The plane wave cut-off energy for the optimized structure was achieved at 35Ry while the Monkhorst-Pack scheme [17] K-points sampling of the Brillouin zone was achieved at $12 \times 12 \times 1$. The plane wave energy cut-off and the k points convergence are shown in Fig. 2 and 3. As regards the doping of stanene with phosphorus and sulfur, since the stanene sheet is made up of 8 atoms it implies that each atom of Sn contributes 12.5% of its effect to the stanene layer. We decided to substitute each of the atoms with a phosphorus (P) atom and that of Sulfur (S), to change the electronic configuration of the stanene sheet at various percentages of 12.5% (1 atom of P/S), 25.0% (2 atoms of P/S), 37.5% (3 atoms of P/S), and 50.0% (4 atoms of P/S) respectively. The structural model of pure and doped stanene nanosheets was viewed via XCRYSDEN software.

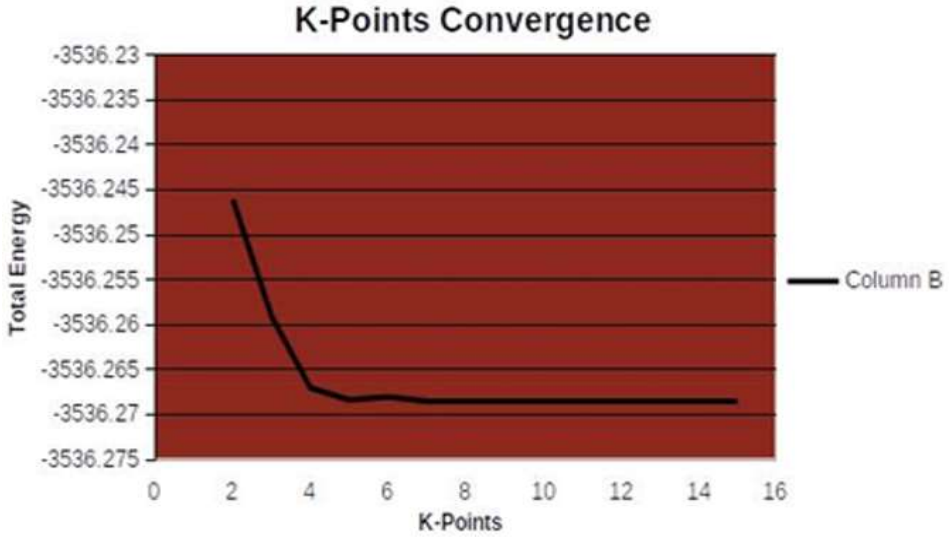


Fig. 2 K-points optimization.

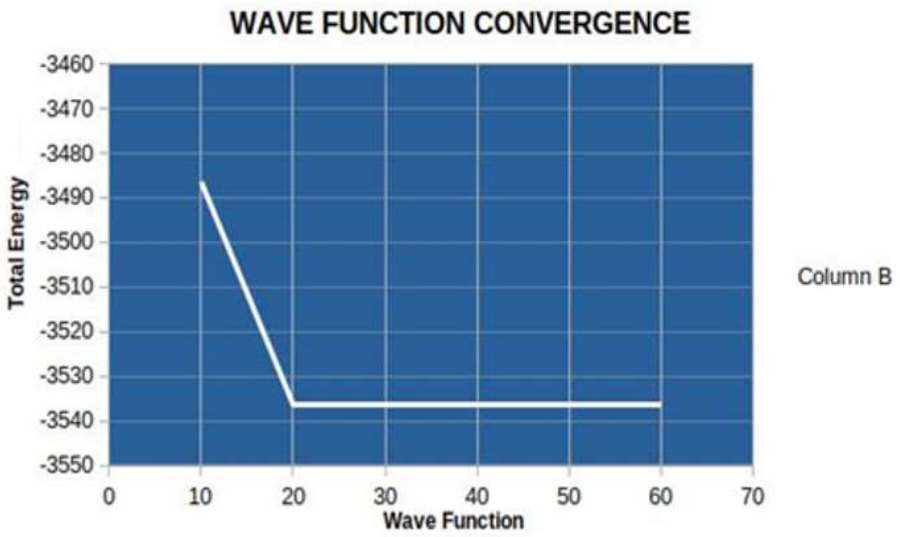


Fig. 3 Wave function optimization.

## IV. RESULTS AND DISCUSSIONS

### *A. Optimized structure of stanene*

In this study, a 2D hexagonal structure of stanene is considered, before doping stanene, The relax and variable cell relax computation was carried out to obtain optimized structural parameters of $a = b =$ 4.67 Å, the volume of the unit cell is 7680.1586 $(a.u.)^3$, the bond length and the bond angle between Sn-Sn atoms are 2.83 Å and 111.6° which is in close agreement with a previously reported value of $a = b =$ 4.68 Å for lattice parameter and 2.83 Å for the Sn-Sn bond length respectively [18]–[21]. The buckling height was investigated to be 0.84 Å and this is in good agreement with the previously reported value of 0.87 Å [12].

### *B. Electronic properties of stanene, stanene-doped phosphorus, and stanene-doped sulfur*

The band structure serves as the diagram where information regarding electronic properties can be extracted. Fig. 4 which depicts the band structure of pristine stanene, shows the zero-band gap nature of stanene with Dirac cones located at the k points, and the fermi level set to zero. Fig. 5 shows the band structure of stanene with the inclusion of the spin-orbit coupling (SOC) effect. When the SOC effect was included, the band gap opened to approximately 0.07 eV. this result is in line with the previously reported study of including the spin-orbit coupling effect in the electronic structure calculation of pristine stanene. [22]–[24].

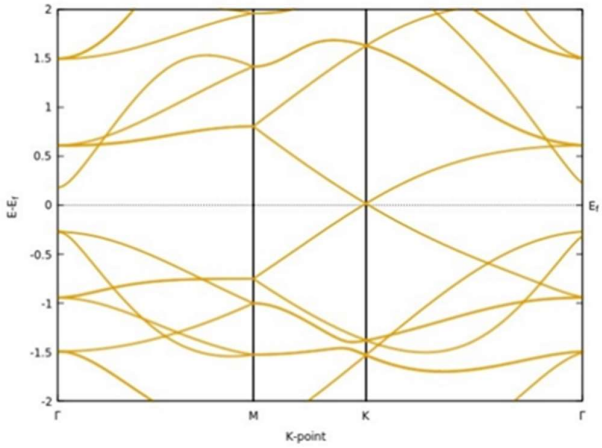


Fig. 4 Band structure of pristine stanene.

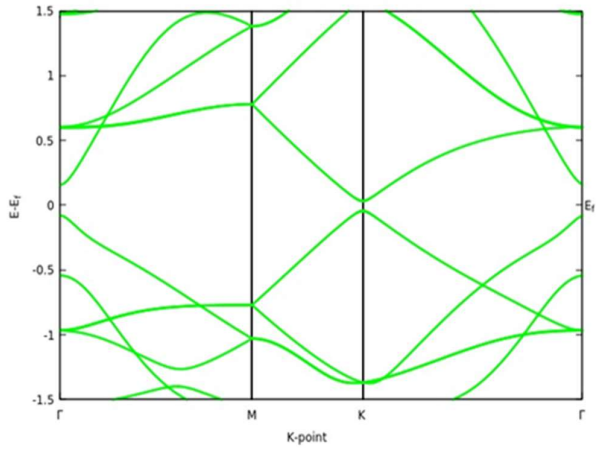


Fig. 5 Band structure of stanene with SOC effect.

Fig. 6 shows the optimized band structure of stanene doped with 1 phosphorus atom (i.e., 12.5%). The band gap opened by 0.26 eV and still maintains its direct band gap shape. Fig. 7 shows the optimized structure of stanene doped with 2 phosphorus atoms (i.e., 25.0%). It maintains its direct band gap and further opens to 0.47 eV. Fig. 8 shows the optimized structure of stanene doped with 3 atoms of phosphorus (i.e., 37.5%). Here, the band gap deteriorates to 0.23 eV, and slightly loses its direct band gap. Fig. 9 The structure is that of stanene doped with 4 atoms of phosphorus (i.e., 50.0%), the material completely loses its semiconducting property. While Fig. 10 to 13 shows the optimized structures and their band gaps for stanene-doped sulfur. Band gap openings of 0.49 eV, 0.77 eV, 0.58 eV, and 0.57 eV were observed for 12.5%, 25.0%, 37.5%, and 50.0% sulfur doping into stanene respectively. Moreover, it is worth noting that, stanene doped with phosphorus and stanene-doped sulfur, gives rise to an n-type material, as the fermi level shifts from its zero position and moves to the conduction band edge.

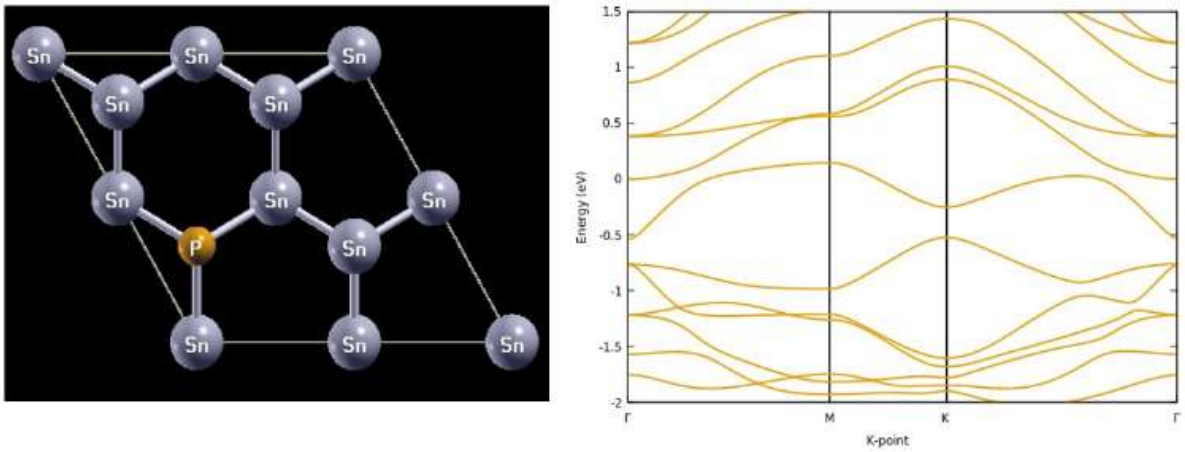


Fig. 6 Doped stanene structure ($SnP_{12.5\%}$) and its band structure ($SnP_{12.5\%}$)

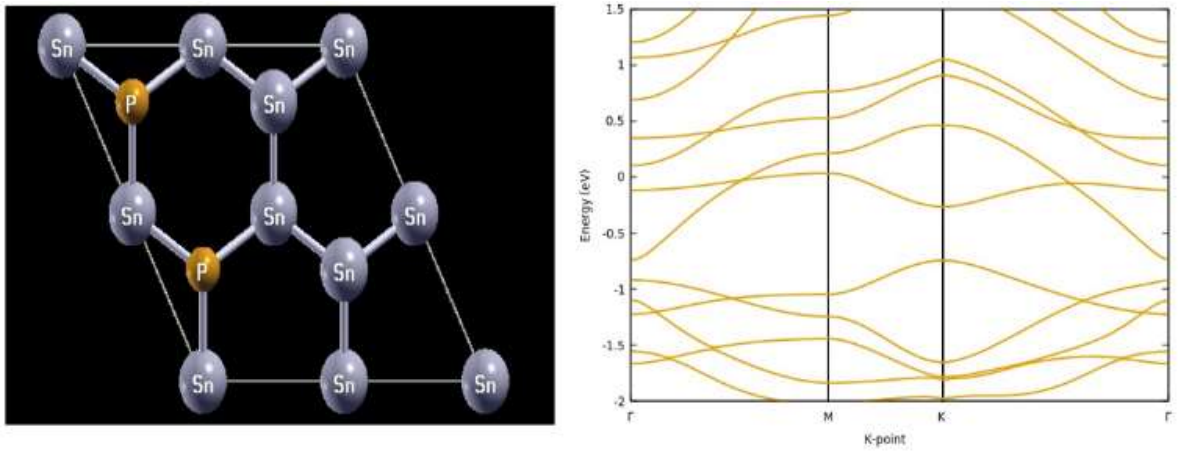


Fig. 7 Doped stanene structure ($SnP_{25.0\%}$) and its band structure ($SnP_{25.0\%}$).

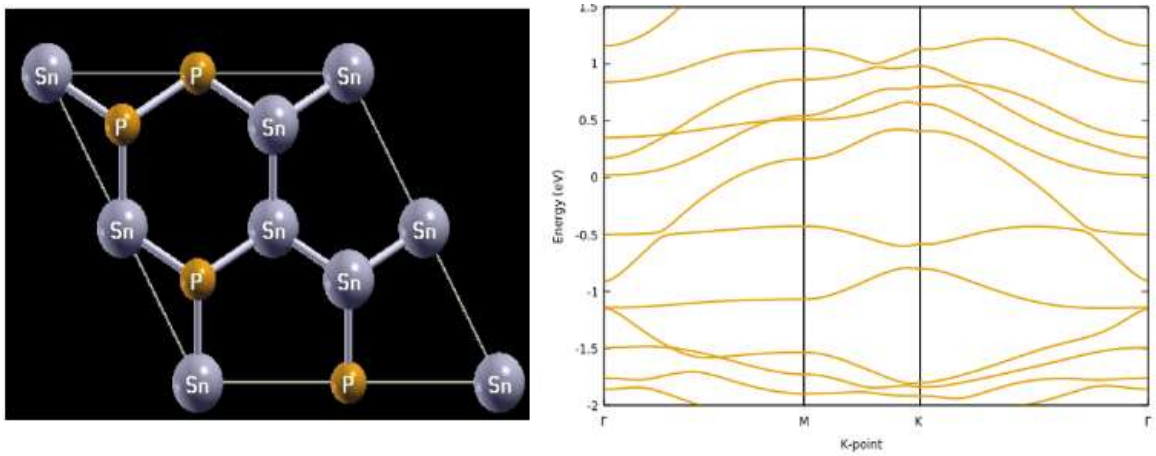


Fig. 8 Doped stanene structure ($SnP_{37.5\%}$) and its band structure ($SnP_{37.5\%}$).

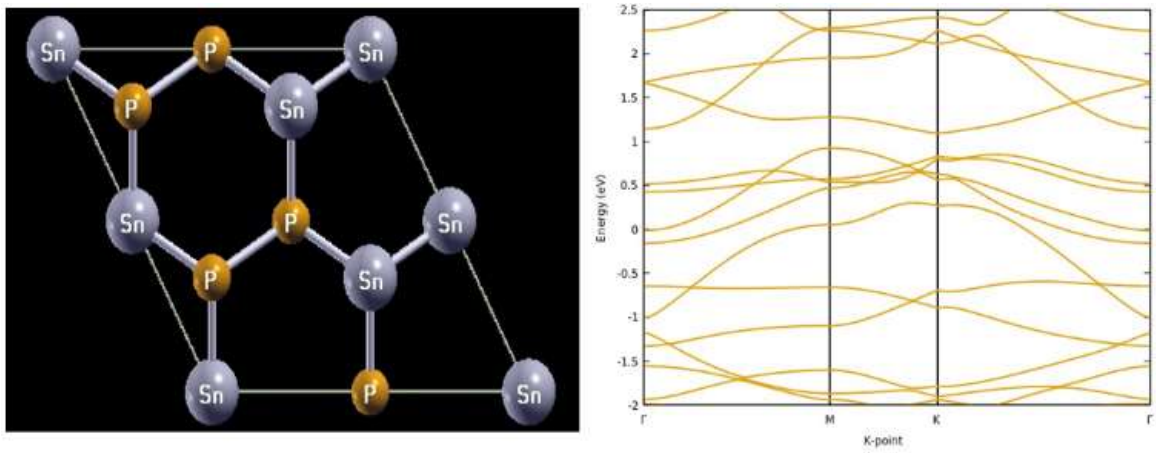


Fig. 9 Doped stanene structure ($SnP_{50.0\%}$) and its band structure ($SnP_{50.0\%}$).

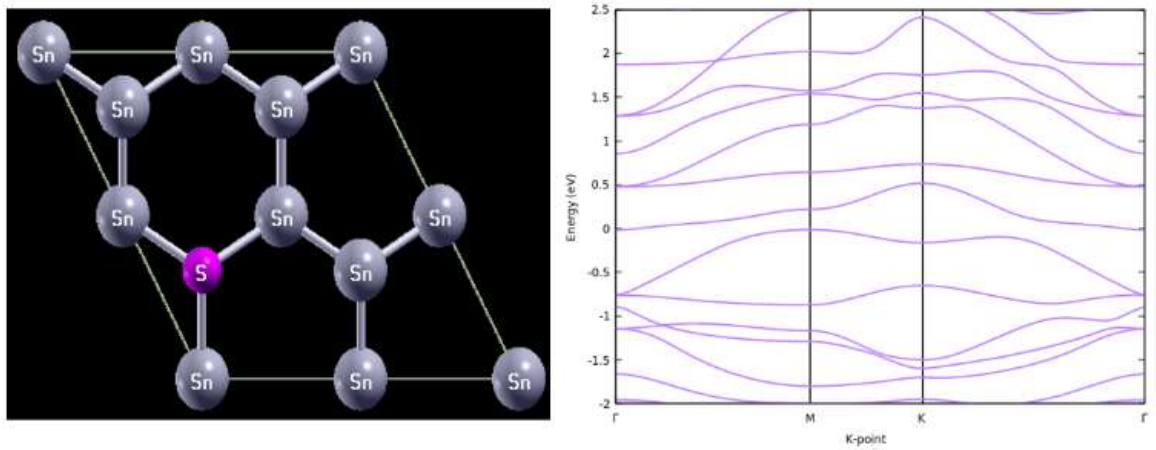


Fig. 10 Doped stanene structure ($SnS_{12.5\%}$) and its band structure ($SnS_{12.5\%}$).

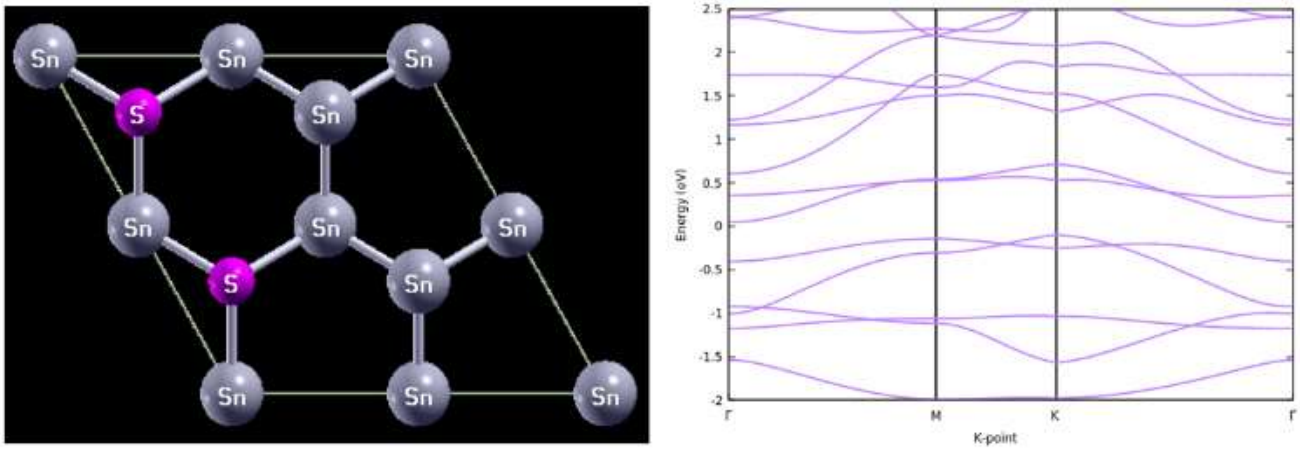


Fig. 11 Doped stanene structure ($SnS_{25.0\%}$) and its band structure ($SnS_{25.0\%}$).

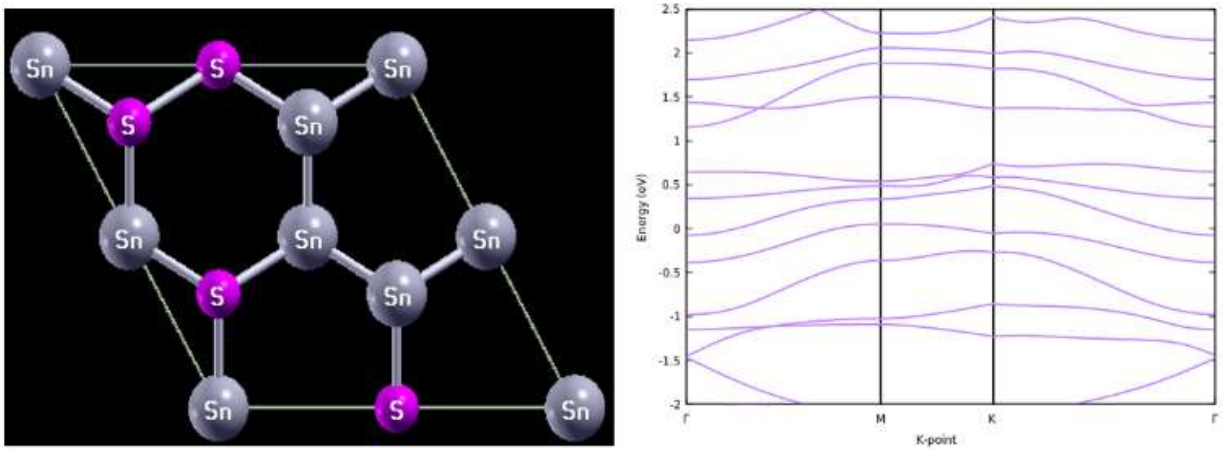


Fig. 12 Doped stanene structure ($SnS_{37.5\%}$) and its band structure ($SnS_{37.5\%}$).

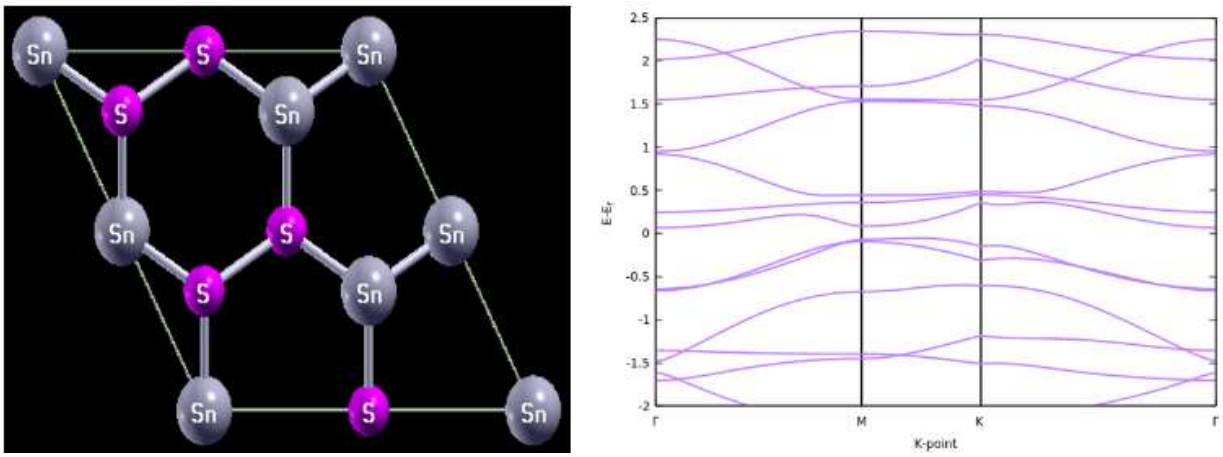


Fig. 13 Doped stanene structure ($SnS_{50.0\%}$) and its band structure ($SnS_{50.0\%}$).

 

### *C. Optical properties of stanene, stanene-doped phosphorus, and stanene-doped sulfur*

The optical properties are also influenced, as the electronic properties of pristine stanene get modified by doping with phosphorus and sulfur respectively. To study the exact effect of doping on optical properties, we computed the optical properties of pristine stanene and compared them with those of stanene-doped phosphorus and stanene-doped sulfur. The dielectric constant (real '$\epsilon$1' and imaginary '$\epsilon$2'), and the electron energy loss function are investigated via random phase approximation (RPA) and the Perdeu-Burke Enzerhof (DFT + RPA) as implemented in the YAMBO code. other optical properties such as reflectivity, refractive index, and extinction coefficient are calculated using the real and imaginary part of the dielectric function given below.

$$\mathrm{n}(w) = \left[\sqrt{\epsilon_1^2(w) + \epsilon_2^2(w)} + \frac{\epsilon_2(w)}{2}\right]^{1/2} \quad (9)$$

$$K(w) = \left[\sqrt{\epsilon_1^2(w) + \epsilon_2^2(w)} - \frac{\epsilon_2(w)}{2}\right]^{1/2} \quad (10)$$

$$R = \frac{(\mathrm{n}-1)^2 + K^2}{(\mathrm{n}+1)^2 + K^2} \quad (11)$$

n(w) is the refractive index, K(w) is the extinction coefficient, R is the reflectivity, $\epsilon_1$(w) is the real part of the dielectric function, $\epsilon_2$(w) is the imaginary part of the dielectric function.

#### *1) Dielectric function and the electron energy loss spectroscopy (EELS)*

The dielectric function for pristine stanene and stanene-doped phosphorus are shown in Fig. 14 to 16, Fig. 17 to 19 while that of stanene-doped sulfur is shown in Fig. 20 to 22. The imaginary part of the dielectric function corresponds to the absorption effect, the real part corresponds to that of the dispersive effect and the electron energy loss function describes the interaction of electrons and solids which is essential for the evaluation of inelastic scattering of electron transport in solids. The absorption effect for pristine stanene peaked at 0.19 eV, its dispersive effect peaked at 0.08 eV, while the EELS is observed at 4.54 eV. As for the stanene-doped phosphorus, the absorption effect peaked at 0.24 eV, 0.13 eV, 0.34 eV, and 0.18 eV for $SnP_{12.5\%}$, $SnP_{25.0\%}$, $SnP_{37.5\%}$, and $SnP_{50.0\%}$ respectively. The dispersive effect was observed at 0.13 eV, 0.08 eV, 0.01 eV, and 0.08 eV for $SnP_{12.5\%}$, $SnP_{25.0\%}$, $SnP_{37.5\%}$, and $SnP_{50.0\%}$ respectively. The EELS were observed to peak at 4.11 eV, 3.95 eV, 3.90 eV, and 3.69 eV for $SnP_{12.5\%}$, $SnP_{25.0\%}$, $SnP_{37.5\%}$, and $SnP_{50.0\%}$. As for the stanene-doped sulfur, the absorption effect peaked at 0.31 eV, 0.68 eV, 0.43 eV, and 0.43 eV for $SnS_{12.5\%}$, $SnS_{25.0\%}$, $SnS_{37.5\%}$, and $SnS_{50.0\%}$ respectively. The dispersive effect was observed to peak at 0.30 eV, 0.42 eV, 0.30 eV, and 0.18 eV for $SnS_{12.5\%}$, $SnS_{25.0\%}$, $SnS_{37.5\%}$, and $SnS_{50.0\%}$ respectively. The EELS were observed to peak at 4.00 eV, 4.00 eV, 3.61 eV, and 8.00 eV for $SnS_{12.5\%}$, $SnS_{25.0\%}$, $SnS_{37.5\%}$, and $SnS_{50.0\%}$.

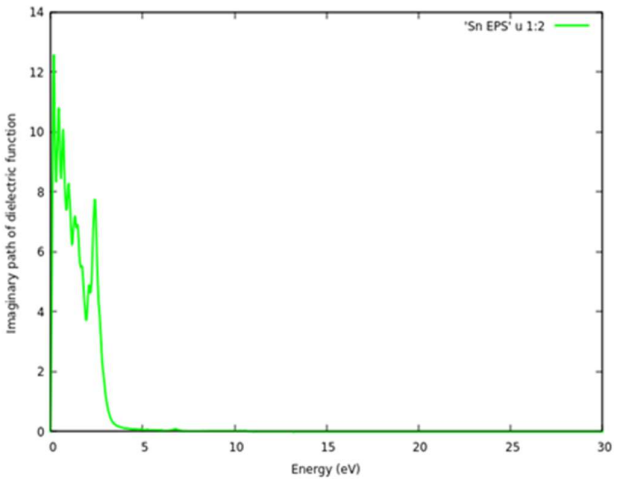


Fig. 14 Imaginary part of dielectric for stanene.

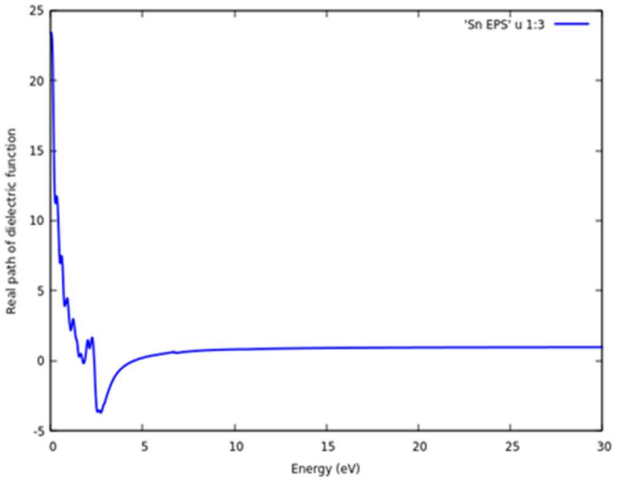


Fig. 15 Real part of dielectric for stanene.

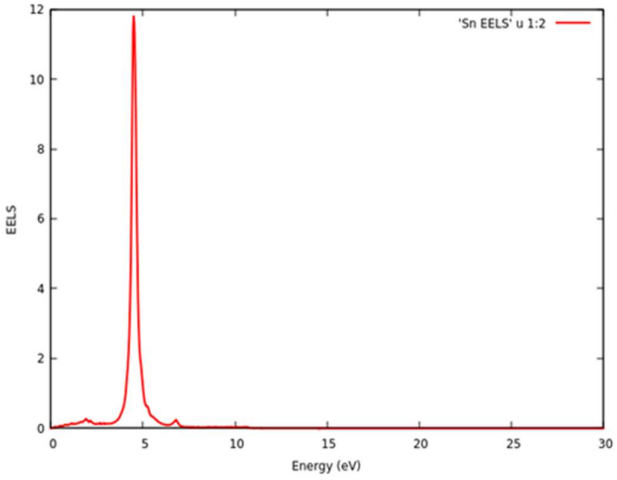


Fig. 16 EELS for stanene.

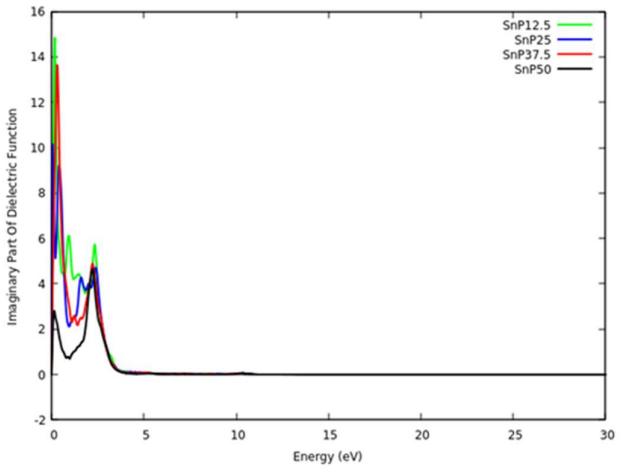


Fig. 17 Imaginary part of the dielectric function.

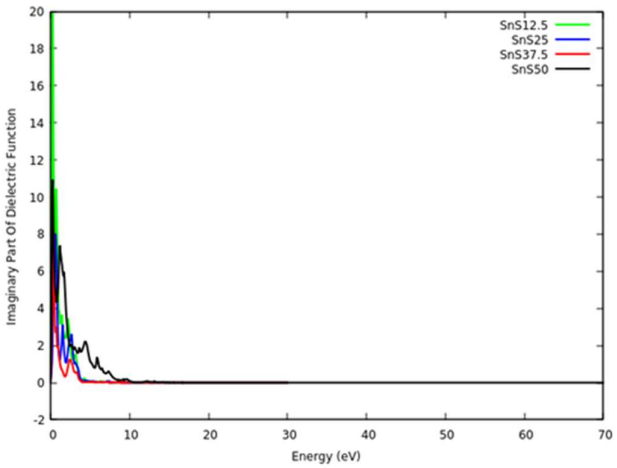


Fig. 20 Imaginary part of the dielectric function.

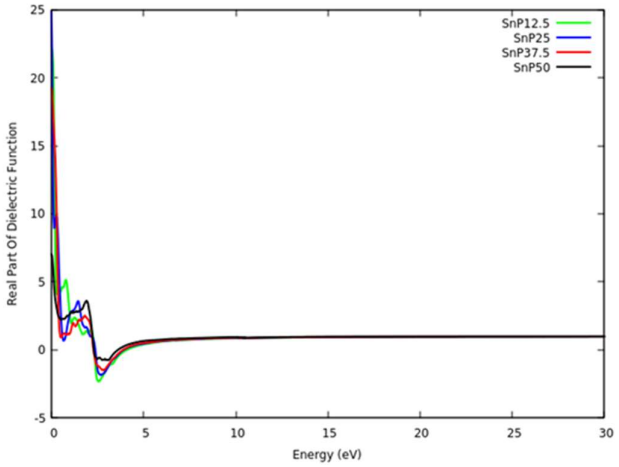


Fig. 18 Real part of the dielectric function.

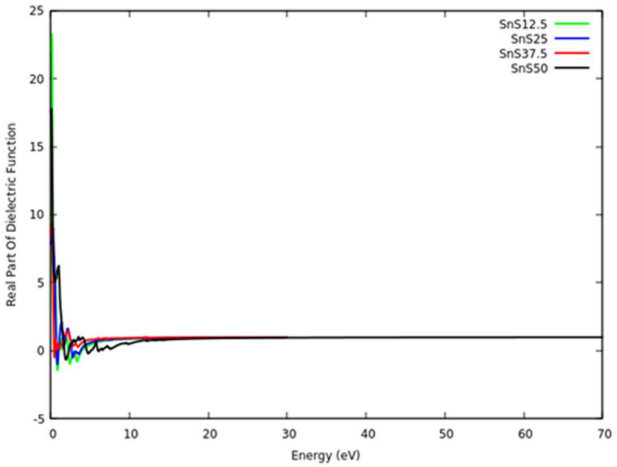


Fig. 21 Real part of the dielectric function.

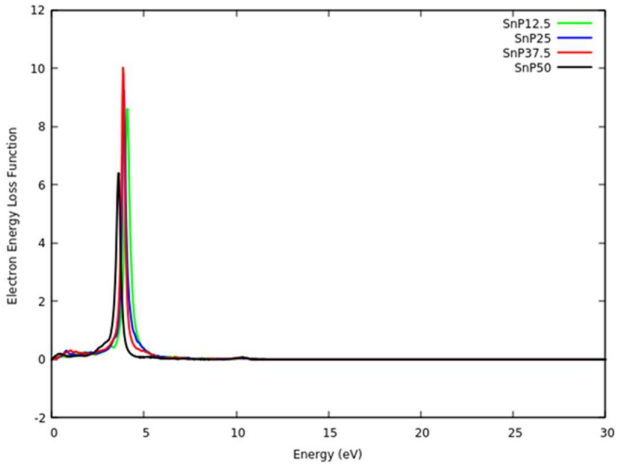


Fig. 19 EELS.

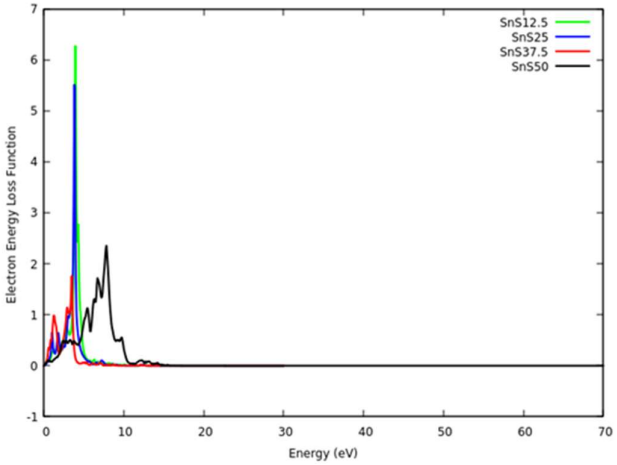


Fig. 22 EELS.

*2) Refractive index and reflectivity*

It is important to investigate the refractive index of a material concerning the designing and modelling of semiconductor devices. High refractive index materials have a great impact on optoelectronic applications. The refractive index and the reflectivity of pristine stanene, stanene-doped phosphorus, and stanene-doped sulfur are shown in Fig.23 to 25 The refractive index for pure stanene is 5.03, that of $SnP_{12.5\%}$, $SnP_{25.0\%}$, $SnP_{37.5\%}$, and $SnP_{50.0\%}$, are 5.49, 5.36, 5.02, and 2.93 respectively. While that of $SnS_{12.5\%}$, $SnS_{25.0\%}$, $SnS_{37.5\%}$, and $SnS_{50.0\%}$ are 5.73, 3.45, 3.67, and 4.66 respectively. The refractive index of $SnP_{12.5\%}$ and $SnS_{12.5\%}$ are higher in comparison to that of stanene and other doping concentrations.

Reflectivity describes the amount of light reflected by a material to that incident on it. Reflectivity is one of the important optical properties of a material. Fig. 26 to 28 shows the variation in reflectivity of stanene, stanene-doped phosphorus, and stanene-doped sulfur. Several peaks appear in the reflectivity curve up to 5 eV. The highest reflectivity of 64% was observed for stanene at an energy of 0.08 eV. that of $SnP_{12.5\%}$, $SnP_{25.0\%}$, $SnP_{37.5\%}$, and $SnP_{50.0\%}$ attains values of 65%, 67%, 63% and 48% at an energy value of 0.03 eV, 0.03 eV, 0.03 eV and 0.03 eV respectively. While for $SnS_{12.5\%}$, $SnS_{25.0\%}$, $SnS_{37.5\%}$, and $SnS_{50.0\%}$ values were observed at 65%, 50%, 51%, and 62% at an energy value of 0.19 eV, 0.31 eV, 0.31 eV, and 0.19 eV respectively.

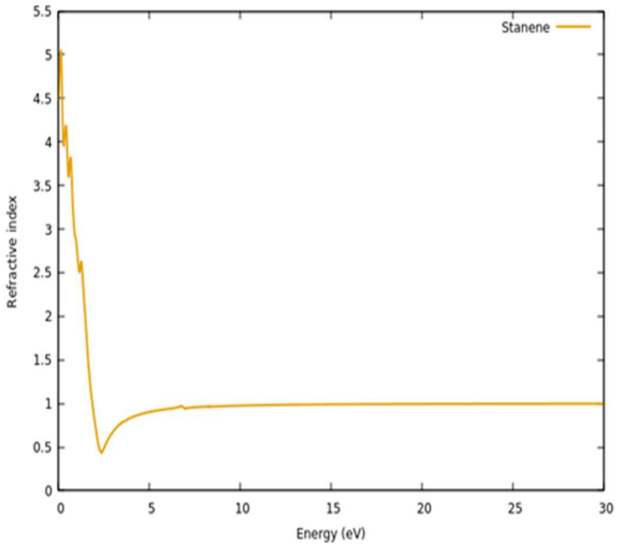


Fig. 23 Refractive index of stanene.

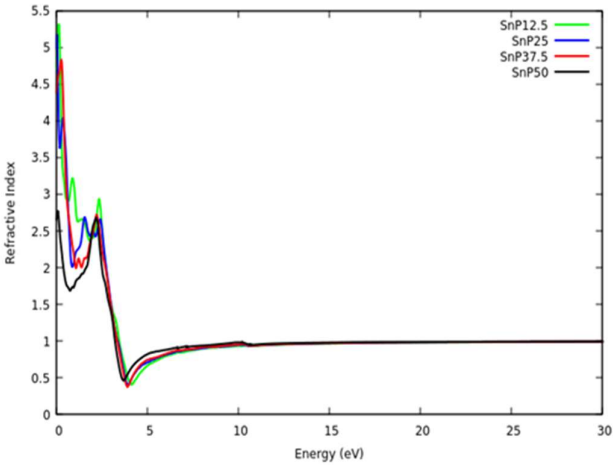


Fig. 24 Refractive index of stanene-doped phosphorus.

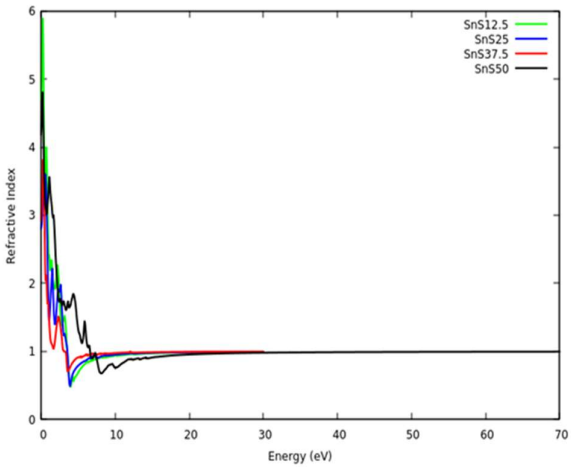


Fig. 25 Refractive index of stanene-doped sulfur.

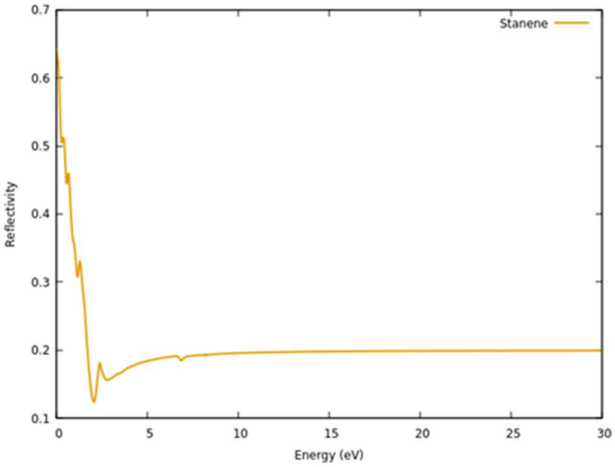


Fig. 26 Reflectivity of stanene.

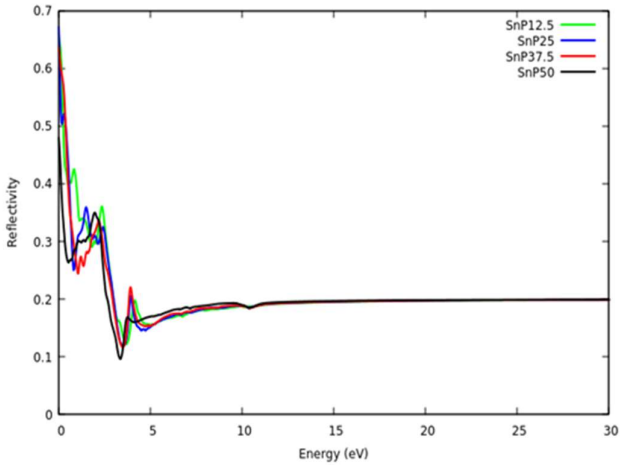


Fig. 27 Reflectivity of stanene-doped phosphorus.

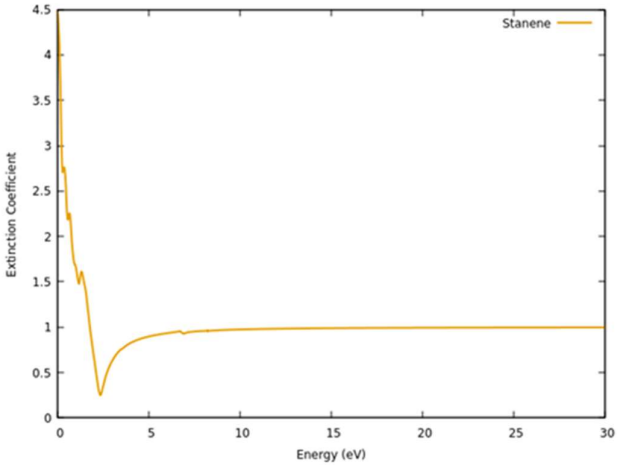


Fig. 29 Extinction coefficient of stanene.

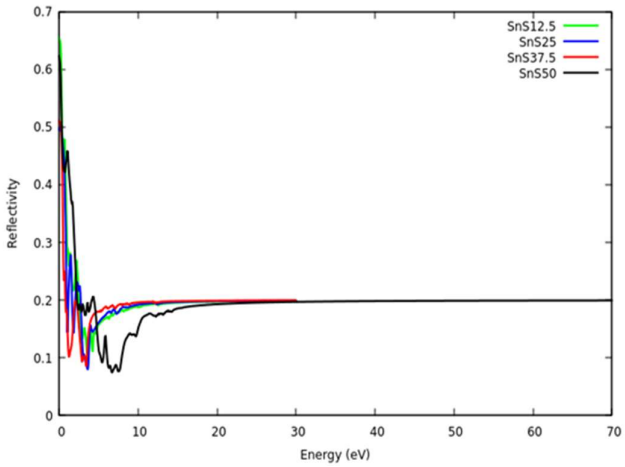


Fig. 28 Reflectivity of stanene-doped sulfur.

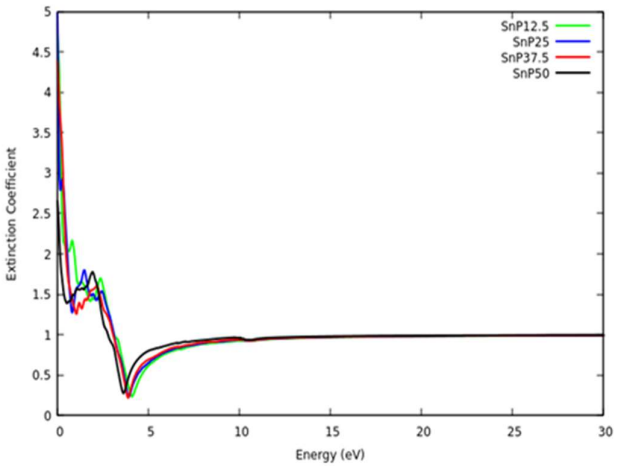


Fig. 30 Extinction coefficient of stanene doped- phosphorus.

*3) Extinction Coefficient*

The mass attenuation or extinction coefficient gives the total effect of a medium on radiation passing through it. Furthermore, it is the sum of the absorption and scattering of radiation into the medium. Fig. 29 to 31 shows the extinction coefficient variation for stanene, stanene-doped phosphorus, and stanene-doped sulfur respectively. After doping stanene, it can be inferred that the extinction coefficient gets lower as the doping concentration increases. However, as the attenuation coefficient decreases, radiations from the flame zone escape to the surrounding.

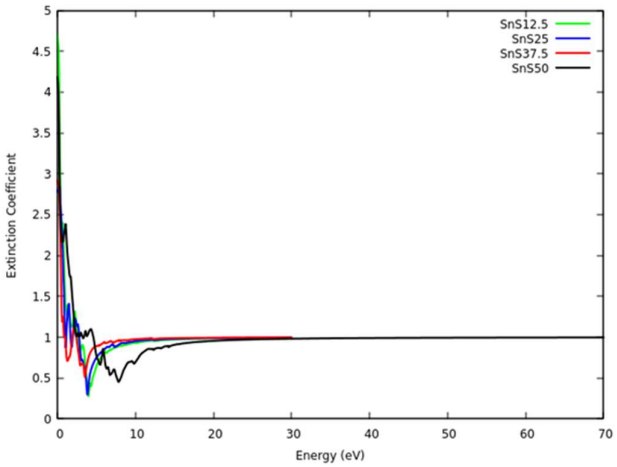


Fig. 31 Extinction coefficient of stanene-doped sulfur.

## V. Conclusion

Through the first principle study, the linearized optical and electronic properties such as band gap, dielectric function, electron energy loss spectroscopy, reflectivity, refractive index, and the extinction coefficient for pristine stanene, stanene doped phosphorus and stanene doped sulfur have been studied respectively. To effectively analyze their optical behavior, we plotted various variations of optical properties against their energies respectively. The pristine stanene exhibits zero band gap. However, with the inclusion of spin to orbit coupling effect, the band gap opened to about 0.07 eV approximately. The band gap of stanene-doped phosphorus and stanene-doped sulfur opened at various doping concentrations with the highest being at 0.47 eV for $SnP_{25.0\%}$ and 0.78 eV for $SnS_{25.0\%}$. A close observation of the optical properties of stanene-doped phosphorus and that of sulfur at various doping concentrations infers that the material exhibits anisotropic behavior. The refractive index of stanene-doped phosphorus and that of sulfur at $SnP_{12.5\%}$ and $SnS_{12.5\%}$ are higher than that of pristine stanene. Thus, $SnP_{12.5\%}$, $SnP_{25.0\%}$, $SnS_{12.5\%}$, and $SnS_{25.0\%}$ could be a promising candidate for optoelectronic applications.

## Reference


[1] W. Pang *et al.*, "Epitaxial growth of honeycomb-like stanene on Au(111)," *Appl. Surf. Sci.*, vol. 517, no. March, pp. 146224, 2020, doi: 10.1016/j.apsusc.2020.146224.

[2] P. Li, "Stanene on a SiC(0001) surface: A candidate for realizing quantum anomalous Hall effect," *Phys. Chem. Chem. Phys.*, vol. 21, no. 21, pp. 11150–11157, 2019, doi: 10.1039/c9cp01509d.

[3] Y. Shaidu and O. Akin-Ojo, "First-principles predictions of superconductivity in doped stanene," *Comput. Mater. Sci.*, vol. 118, pp. 11–15, 2016, doi: 10.1016/j.commatsci.2016.02.029.

[4] R. Ahmed, T. Nakagawa, and S. Mizuno, "Structure determination of ultra-flat stanene on Cu(111) using low energy electron diffraction," *Surf. Sci.*, vol. 691, no. September 2019, pp. 121498, 2020, doi: 10.1016/j.susc.2019.121498.

[5] A. I. Khan, T. Chakraborty, N. Acharjee, and S. Subrina, "Stanene-hexagonal boron nitride heterobilayer: Structure and characterization of electronic property," *Sci. Rep.*, vol. 7, no. 1, pp. 1–10, 2017, doi: 10.1038/s41598-017-16650-5.

[6] J. K. Lyu, S. F. Zhang, C. W. Zhang, and P. J. Wang, "Stanene: A Promising Material for New Electronic and Spintronic Applications," *Ann. Phys.*, vol. 531, no. 10, pp. 1–12, 2019, doi: 10.1002/andp.201900017.

[7] A. Abbasi and J. J. Sardroodi, "Electronic structure tuning of stanene monolayers from DFT calculations: Effects of substitutional elemental doping," *Appl. Surf. Sci.*, vol. 456, no. March, pp. 290–301, 2018, doi: 10.1016/j.apsusc.2018.06.078.

[8] A. Shrivastava, S. Saini, and S. Singh, "Ab-Initio investigations of electronic and optical properties of Sn-hBN heterostructure," *Phys. B Condens. Matter*, vol. 624, pp. 413390, 2022, doi 10.1016/j.physb.2021.413390.

[9] L. Wu *et al.*, "Structural and electronic properties of two-dimensional stanene and graphene heterostructure," *Nanoscale Res. Lett.*, vol. 11, no. 1, 2016, doi: 10.1186/s11671-016-1731-z.

[10] B. Chakraborty, M. M. Borgohain, and N. C. Adhikary, "Structural and electronic properties of Stanene- BeO heterobilayer," Mater. Res. Express, vol. 7, no. 1, 2019, doi: 10.1088/2053-1591/ab6091, 2020.

[11] S. Ullah, P. A. Denis, and F. Sato, "Beryllium doped graphene as an efficient anode material for lithium-ion batteries with significantly huge capacity: A DFT study," *Appl. Mater. Today*, vol. 9, pp. 333–340, 2017, doi: 10.1016/j.apmt.2017.08.013.

[12] L. S. Taura, I. Abdulmalik, A. S. Gidado, and A. Lawal, "Structural, Electronic and Optical Properties of Stanene Doped Beryllium: A First Principle Study," *Phys. Sci. Int. J.*, pp. 32–40, Aug. 2021, doi: 10.9734/psij/2021/v25i430251.

[13] K. Burke and K. Burke, "Perspective on density functional theory Perspective on density functional theory," vol. 150901, 2012, doi: 10.1063/1.4704546.

[14] D. Bagayoko, "Understanding density functional theory (DFT) and completing it in practice," *AIP Adv.*, vol. 4, no. 12, pp. 0–12, 2014, doi: 10.1063/1.4903408.

[15] P. Giannozzi *et al.*, "QUANTUM ESPRESSO: A modular and open-source software project for quantum simulations of materials," *J. Phys. Condens. Matter*, vol. 21, no. 39, 2009, doi: 10.1088/0953-8984/21/39/395502.

[16] P. Giannozzi *et al.*, "Advanced capabilities for materials modelling with Quantum ESPRESSO," *J. Phys. Condens. Matter*, vol. 29, no. 46, 2017, doi: 10.1088/1361-648X/aa8f79.

[17] K. Hu *et al.*, "Boosting electrochemical water splitting: via ternary NiMoCo hybrid nanowire arrays," *J. Mater. Chem. A*, vol. 7, no. 5, pp. 2156–2164, 2019, doi: 10.1039/c8ta11250a.

[18] X. Chen, Y. Li, J. Tang, L. Wu, D. Liang, and R. Zhang, "First-principles study on electronic properties of stanene/WS2monolayer," *Mod. Phys. Lett. B*, vol. 31, no. 29, pp. 1–12, 2017, doi: 10.1142/S0217984917502712.

[19] Zhu, F. et al., "Epitaxial growth of two-dimensional stanene". Nat. Mat., vol. 14, no. 10, 2015, pp. 1020–1025. doi:10.1038/nmat4384.

[20] S. Saxena, R. P. Chaudhary, and S. Shukla, "Stanene: Atomically Thick Free-standing Layer of 2D Hexagonal Tin," *Sci. Rep.*, vol. 6, pp. 1–4, 2016, doi: 10.1038/srep31073.

[21] H. Shinotsuka, H. Yoshikawa, and S. Tanuma, "First-principles calculations of optical energy loss functions for 30 compound and 5 elemental

semiconductors," *e-Journal Surf. Sci. Nanotech.*, vol. 19, pp. 70–87, 2021, doi: 10.1380/EJSSNT.2021.70.

[22] A. Abbasi, "DFT study of the effects of Al–P pair doping on the structural and electronic properties of stanene nanosheets," *Phys. E Low-Dimensional Syst. Nanostruct.*, vol. 108, no. May 2018, pp. 34–43, 2019, doi: 10.1016/j.physe.2018.12.012.

[23] M. Ghezali, B. Amrani, Y. Cherchab, and N. Sekkal, "Structural and electronic properties of LaN," *Mater. Chem. Phys.*, vol. 112, no. 3, pp. 774–778, 2008, doi: 10.1016/j.matchemphys.2008.06.031.

[24] A. Shuaibu, Y. Tanko, Z. Abdurrahman, A. Lawal, and M. Nasir, "Effect of Beryllium and Magnesium Doped Stanene Single Layer on Structural and Electronic Properties Using Density Functional Theory as Implemented in Quantum ESPRESSO," *Phys. Access*, vol. 01, no. 01, pp. 1–7, 2021, doi: 10.47514/phyaccess.2021.1.1.001.